No-Flow Temperature in Injection Molding Simulation

G. A. Mannella,[1] V. La Carrubba,[1] V. Brucato,[1] W. Zoetelief,[2] G. Haagh[2]

[1]*Dipartimento di Ingegneria Chimica dei Processi e dei Materiali, Università di Palermo, Palermo 90128, Italy*
[2]*DSM Research - P.O. Box 18, 6160 MD, Geleen, The Netherlands*

Received 15 April 2010; accepted 19 June 2010
DOI 10.1002/app.32987
Published online 29 September 2010 in Wiley Online Library (wileyonlinelibrary.com).

ABSTRACT: Most injection molding simulation packages use the no-flow temperature (NFT) as a means of determining whether the polymer flows or is solid. The NFT is not well defined, and a standard method for measuring it does not exist. A sensitivity analysis of the filling stage has been carried out with two different packages [VISI Flow (Vero Software Limited, Gloucestershire, UK) and Moldflow (Autodesk, Inc., San Rafael, CA)] to estimate the influence of the NFT on the main processing parameters. The NFT has a large influence on the thickness of the frozen layer, but it does not appreciably affect the filling pressure. Because the NFT affects the frozen layer, an effect on the estimation of shrinkage and warpage is expected. Software packages have also been compared, and similar simulations have been found to produce contrasting results. A simple correlation for NFT estimation, derived from the Cross–Williams–Landel–Ferry equation, is proposed for both amorphous and semicrystalline polymers. © 2010 Wiley Periodicals, Inc. J Appl Polym Sci 119: 3382–3392, 2011

Key words: injection molding; processing; simulations

INTRODUCTION

Polymer solidification is a key point in the injection-molding process because it takes place throughout the entire process with different dynamics and affects the final properties of the product.

During injection molding, a polymer experiences a complex thermomechanical history that determines the final morphology. Morphology prediction is a challenge for injection molding simulation packages, and to reach this objective, an accurate estimate of solidification dynamics is needed.

At present, the development of an experimental method to accurately and reliably measure the solidification kinetics during injection molding (with a particular emphasis on the filling stage) is still an open task. A capacitance transducer has been proposed[1] to measure the flow-front position and the rate of solidification during the holding/packing stage. Another noninvasive tool is the ultrasonic technique,[2] which allows real-time process monitoring. The indentation test,[3] which needs an offline measure, is a tool for monitoring solidification during the holding stage.

A recent approach to the liquid–solid transition of semicrystalline polymers uses the gelation concept.[4] Gelation is related to changes in physical and rheological properties due to chemical (or physical) crosslinking reactions of polymers, which increase connectivity. During crystallization, large-scale connectivity between polymer chains is established; therefore, crystallization can be treated as a physical gelation process. The liquid–solid transition then occurs at the physical gel point. Stress during crystallization has a double effect. It increases the rate of crystallization and thus the number of physical bonds. However, it also breaks up physical clusters, so the solidlike behavior at the gel point depends on the experimental times. At the gel point, the physical gel is still a liquid if stress is applied for times longer than the maximum relaxation time of the physical gel.

Gelation occurs during the very early stages of crystallization, and for isotactic polypropylene, a relative crystallinity of approximately 2% or less at the gel point was found,[5] although this value was corrected (to 12–17%) in later publications.[6]

How a low level of crystallinity is related to a liquid–solid transition is still unclear, and the microstructure involved in gelation still needs to be explained thoroughly.[7] Progress in studies about physical gelation is expected for both theoretical issues (e.g., gel structure and rheology over a wide range of frequencies) and experimental issues (e.g., accurate gel point detection and influence of the cooling rate).

Another way of relating rheological properties to crystallinity involves comparing differential scanning calorimetry (DSC) and dynamic mechanical analysis (DMA) results achieved with the same thermal history. A good correlation between the viscosity and crystallinity was found for isotactic polypropylene, and

Correspondence to: V. La Carrubba (lacarrubba@dicpm.unipa.it).

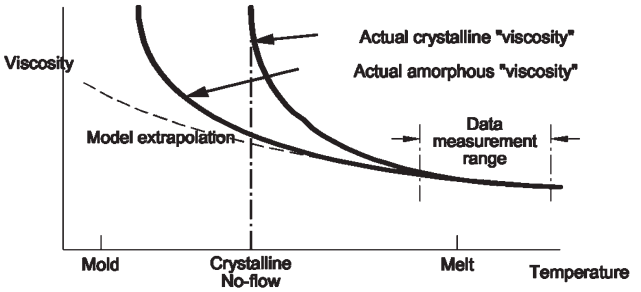

Figure 1 Comparison of the model prediction and the actual viscosity (from ref. 13).

a master-curve approach was proposed to relate the hardening of a polymer to its crystallinity[8] and hence to describe the viscosity increase with crystallization. Acierno et al.[9] proposed a model to relate the induction time of crystallization to the temperature and shear rate, the main parameters affecting viscosity.

An enhancement factor was adopted by Titomanlio et al.[10] to describe the effect of crystallinity on viscosity, and from this, a crystallinity solidification index (CSI) was derived. The crystallinity solidification index is the crystallinity value at which the viscosity increases by 1 order of magnitude at a constant temperature.

Because of the aforementioned complexity, commercial injection-molding simulation software packages use the oversimplified no-flow temperature (NFT) concept to treat polymer solidification.

The NFT[11,12] was originally proposed by Moldflow simulation code developers. It is not a well-defined property because it was introduced to simplify calculations of mold filling.[13] Injection molding processing conditions are so far from the conditions of conventional analytical techniques that a different way of figuring out the solidification phenomenon is needed to improve software package predictions. In Figure 1, typical actual and predicted viscosity values are compared. Viscosity measurements are usually performed at high temperatures, and extrapolation dramatically sacrifices accuracy at temperatures close to solidification. For semicrystalline materials, deviations are large because of crystallization, and this greatly modifies the rheological properties of flowing polymers. For amorphous materials, deviations are generally lower; nevertheless, in this case as well, the use of the NFT concept can enhance the accuracy level.

A schematic of the NFT use in injection molding simulations refers to the polymer velocity (v):

$$v(x,y,z) = \begin{cases} 0 & T \leq \text{NFT} \\ v & T > \text{NFT} \end{cases} \quad (1)$$

where T is the temperature. The NFT is in some ways an empirical rheological solidification temperature for which viscosity models at present do not account. There are several possibilities for defining the NFT:

1. First and simply, the NFT is the temperature below which a polymer will not flow.[14] Therefore, the NFT somehow provides a measure of the solidification temperature of the melt,[15] and it is frequently different from the melting temperature (T_m), crystallization temperature (T_c), and glass-transition temperature (T_g). These characteristic temperatures depend on the heating/cooling rate[16] and pressure.[17] Under standard conditions (cooling rate, $\dot{T} = -10$–20°C/min, DSC), $T_m - T_c$ is approximately 50–60°C. The NFT is usually higher than T_g. For practical purposes, in many simulation examples, it has been assumed to be $T_g + 30$°C.[18] A typical range of NFT values for amorphous polymers is 20–70°C above T_g, whereas, because of supercooling, ranges of NFT values for semicrystalline plastics are usually 10–80°C below T_m (depending on the crystallization behavior).[19]
2. A more physically grounded definition of the NFT focuses on the observation that at the NFT, the melt reaches a viscosity so high that it cannot proceed further, but it has not yet fully solidified as a result of vitrification or crystallization.[20,21]
3. For semicrystalline polymers, it is more difficult to relate the NFT to physical phenomena because of the complexity of the crystallization kinetics, the influence of the formation of crystals and their size distribution on the fluid dynamics, and the mutual influence of flow and crystallization.[22] In this respect, for a given polymer, different levels of shear at different shear rates will generate a vast range of crystalline morphologies that can locally lead to different NFTs. Although a more appropriate definition is still desirable, the NFT concept is applicable even to semicrystalline materials. Furthermore, to fully incorporate the crystallization, the thermomechanical history has to be taken into account (e.g., as described by Kennedy[23]).

This variety of definitions shows the lack of theoretical studies on the NFT.

With the aforementioned empirical concept of the NFT, a fluid is subdivided into a frozen layer and a fluid layer. Thus, semicrystalline and amorphous polymers can be treated similarly.[24] Moreover, with an empirical estimate of melt stopping, the use of the NFT can improve predictions of short shots.

Although the NFT overcomes some simulation problems, the addition of this new variable introduces errors into calculations because of its unclear definition, unfocused phenomenology, and scarcely

unified measure. A rigid distinction between the solid and melt states becomes critical in thin-wall simulations, in which small errors in frozen layer estimation strongly influence pressure-drop predictions because the frozen-layer fraction in thin-walled parts is much larger. Moreover, for semicrystalline polymers, a viscosity cutoff is not sufficient to obtain good predictions because the influence of crystallization on viscosity is not explained by the models so far used in software packages. Because different NFT values are used for the same material in different software packages, the NFT can become an adjustable parameter to fit simulations to experimental data.

All things considered, the NFT concept reflects in some way the basic phenomenology occurring during mold filling, and although it does not configure as a fundamental physical property of a material, it is incorporated into a number of common injection-molding flow analysis software packages.[13] To improve the predictive quality of simulations, a more appropriate definition and measure of the NFT, possibly coupled with more accurate and reliable viscosity models, is required.

This study stems from our interest in the injection molding simulation of thin-walled parts. The use of a three-dimensional approach does not allow easy tracking of the solid/fluid interface, which is possible with the 2.5D approach (into which the NFT is incorporated). According to this approach, three dimensions are considered for temperature, whilst only two dimensions for pressure (i.e pressure is assumed to be constant along mold thickness). Because the latter approach also allows a lot of computation time to be saved, an accurate estimation of the parameters (e.g., the NFT) can greatly improve the performance of thin-wall injection molding simulations. The first part of our work is a sensitivity analysis of various parameters of the filling stage via simulations of short shot. The second part is aimed at proposing a simple correlation for NFT estimates for amorphous and semicrystalline polymers.

SENSITIVITY ANALYSIS

The use of injection molding simulation software packages is a way of systematically investigating the effects of the NFT on the filling process. Two different packages were used: Moldflow and VISI Flow (a package distributed by Vero Software). Although the aims of these software packages are similar (i.e., supplying numerical predictions about injection-molding stages and final properties of products), there are many differences between them (e.g., the NFT databases).

Details on calculation methods are not known because commercial codes are protected; therefore, it is possible only to visualize general differences related to parameters and models used to simulate injection molding. A rough parameter for quantifying moldability is the mold length, i.e. the length that can be filled by a molten polymer under a given pressure. This parameter, although it depends on molding conditions, may provide useful information, especially when different materials are being compared. As the NFT is related to the flow-front stop, it is reasonable to try to relate the NFT to the filled length in a short shot. When the calculated temperature distribution in a section falls below the NFT, the simulation result is a short shot.

Another parameter related to moldability is the injection pressure. In an injection molding machine, it is possible to set a maximum filling pressure (P_{max}) to avoid flash formation. Flash is any excess material formed with and attached to the component along a seam or mold parting line. In an injection-molding simulation, as in practice, when P_{max} is reached, the injection velocity cannot be maintained. The effect of NFT variation on the maximum injection pressure cannot be studied directly because P_{max} is reached in all simulations. Nevertheless, the filled length at P_{max} can be considered a measure of the sensitivity of the injection pressure. If the NFT influences the pressure distribution during filling, the length at which P_{max} is reached will change. In our simulations, P_{max} was set to 2000 bar, which is in line with typical injection molding equipment.

The NFT has a direct influence on the frozen-layer fraction, that is, the region in which the temperature is below the NFT. Because the frozen-layer domain is two-dimensional (so it is not easy to compare different distributions), a simpler way of quantifying changes in the frozen-layer fraction is needed to evaluate the sensitivity. In this respect, the length with a frozen-layer fraction between 0 and 10% ($L_{10\%}$) is the zone close to the injection point and represents the region in which only a small amount of the polymer has reached the NFT (see Fig. 2). The use of $L_{10\%}$ despite the two-dimensional distribution allows easier sensitivity analysis without a lack of physical meaning.

This parameter is suitable for this analysis because the frozen-layer fraction increases along the flow direction (with reference to the zone close to the injection point). Therefore, effects of the NFT on the frozen-layer distribution can be related to the length of the first zone.

Methods

To simulate a short shot, a long, rectangular cavity was chosen as the mold. Its length and width were set to 900 and 120 mm, respectively; two different thicknesses (1.2 and 1.5 mm) were investigated because the mold thickness strongly influences energy transport, that is, temperature distributions.

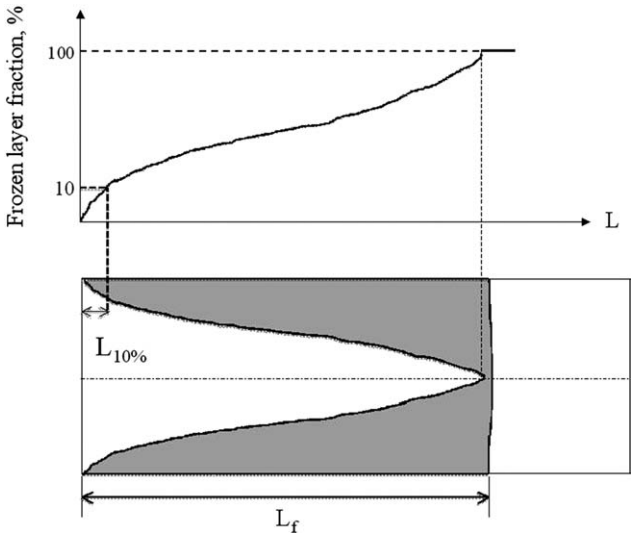

Figure 2 Frozen-layer fraction versus the mold length in a short shot (top) and mold cross section (bottom). L_f is the length filled in the short shot.

The melt temperature (T_{melt}) and the mold temperature (T_{mold}) were taken from the databases of the software packages, which also reported recommended process conditions.

Four different materials were selected to compare the behaviors of materials with very different physical properties (T_m and T_g): two amorphous [polycarbonate (PC) and polystyrene (PS)] and two semicrystalline [poly(butylene terephthalate) (PBT) and polyamide 6 (PA6)]. For semicrystalline polymers, only the 1.2-mm-thick mold was used because the 1.5-mm-thick mold resulted in complete filling under all conditions.

Mold-filling simulations were performed at four different flow-front velocities (0.1, 0.15, 0.2, and 0.3 m/s) to account for different energy dissipation values and energy convective transport contributions. T_{melt} and T_{mold} were selected from the recommended processing conditions reported in the software package databases. The values of T_{melt} and T_{mold} used in the simulations, together with the Cross–Williams–Landel–Ferry (WLF) parameters of the polymers (discussed later), are reported in Table I.

Analyses were performed with VISI Flow software. A set of PA6 filling simulations was performed with Moldflow so that we could compare results.

The input distribution was chosen around the database value of the no-flow temperature (NFT_0; Table II). The investigated range was $NFT_0 - 20°C < NFT < NFT_0 + 40°C$. This interval is not symmetric with respect to NFT_0 because for low NFTs, numerical problems affect simulations, calculations stop, and results are not reliable. For PS analysis, the lower boundary was chosen to be $NFT_0 - 10°C$.

Results and discussion

To effectively compare simulations with respect to the filled length, a relative scaling factor was used. A plot of the filled length (L) scaled with the filled length at NFT_0 (L_0) was used to analyze the results.

Curves at different velocities for PC (Fig. 3) appreciably overlap, so changes in the filled length are related only to the NFT. From NFT = 160°C to NFT = 220°C, the filled length reduction is approximately 20% for both mold thicknesses tested (results for the 1.5-mm-thick mold are not shown here for the sake of brevity).

For all materials tested, the velocity does not appreciably influence the filled length. Conversely, the main influence is exerted by the NFT (Fig. 4). In a general way, L/L_0 decreases with an NFT increase.

For PS, a 50°C increase in the NFT (i.e., from 120 to 170°C) leads to a decrease in the filled length of approximately 38% (mold thickness $h = 1.2$ mm) or 33% ($h = 1.5$ mm, not reported here).

For PA6, a 60°C increase in the NFT (i.e., from 165 to 225°C) produces a 36% reduction in the filled length.

For PBT, unlike the other cases, at low NFTs, minor changes in the filled length are observed. An increase in the NFT from 160 to 200°C reflects a reduction of the filled length of approximately 15%.

The dependence of the filled length on the NFT is fairly influenced by the mold thickness for amorphous materials because the thickness affects only the absolute value of the filled length.

Semicrystalline materials show different behaviors with changes in the NFT. This can be related to the phenomenology occurring with cooling from the melt (e.g., crystallization), but it is not known how these issues are taken into account by the software packages.

TABLE I
T_{melt}, T_{mold}, and Cross–WLF Parameters Used in the Simulations

Polymer	T_{melt} (°C)	T_{mold} (°C)	n	τ^* (Pa)	D_1 (Pa s)	D_2 (K)	A_1	A_2 (K)
PC	300	90	0.1143	8.48×10^5	5.17×10^{11}	417.15	28.039	51.6
PS	200	45	0.3359	3.26×10^3	3.32×10^{12}	373.15	24.27	51.6
PA6	260	65	0.2933	2.19×10^5	4.5×10^{14}	323.15	35.88	51.6
PBT	255	90	0.319	2.11×10^5	1.06×10^{22}	323.15	55.838	51.6

TABLE II
NFT_0 Values of Various Polymers (from VISI Flow)

Polymer	NFT_0 (°C)
PC	180
PS	130
PA6	185
PBT	160

A typical plot of the filled length at P_{max} is reported in Figure 5. Except for PS, this parameter is appreciably insensitive to NFT. This general result can be explained as follows: at higher NFTs, the open-section reduction is compensated by the viscous and convective heating contributions.

The results for PS (Fig. 6) show a dependence on the NFT. The filled length reduces its value with increasing NFT. The influence is higher at a low flow-front velocity, whereas at a high velocity, a constant flow rate can be longer sustained. At $v = 0.3$ m/s, a 50°C increase in the NFT (i.e., from 120 to 170°C) produces a reduction of the filled length at P_{max} of 13% ($h = 1.2$ mm) or 20% ($h = 1.5$ mm). At $v = 0.1$ m/s, the reduction is 40% for both mold thicknesses.

The previously defined $L_{10\%}$ parameter was adopted to estimate the sensitivity of the frozen-layer fraction.

PC results for a 1.2-mm-thick mold (Fig. 7) are similar to the results for the other tested mold thicknesses. All the curves exhibit a constant slope at low NFTs of approximately −4 mm/°C for a 1.2-mm thickness. For a 1.5-mm-thick mold, this slope is approximately −5 mm/°C. At a critical value of the NFT, the slope changes (first increasing and then decreasing), and the length values rapidly approach zero. The velocity influences the position of the critical point (a low velocity shifts it toward a low NFT).

Figure 8 shows results for all materials normalized to the filled length (L_f) at $v = 0.2$ m/s. The PS results can be explained as follows: the explored temperature range lies above the critical temperature because the length falls abruptly to zero. The same consideration is valid for PA6.

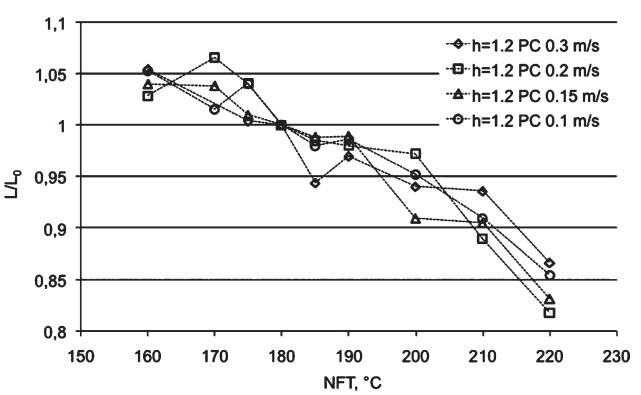

Figure 3 Plot of L/L_0 versus NFT (PC, $h = 1.2$ mm).

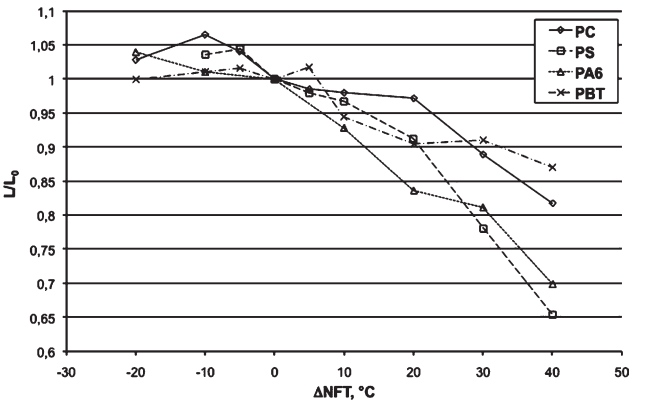

Figure 4 Plot of L/L_0 versus NFT ($v = 0.2$ m/s, $h = 1.2$ mm).

The PBT results are similar to the PC results and show a constant-slope region at low NFTs and a critical temperature at which the length rapidly approaches zero. The slope at low NFTs is approximately −4 mm/°C, that is, the same value for PC with the same mold thickness.

Thickness does not exert a strong influence on all the investigated parameters. The filled length shows a linear dependence on the NFT, except for some low-velocity cases. The filled length at P_{max} does not show an appreciable dependence on the NFT, except for PS. Conversely, a general dependence of $L_{10\%}$ on the NFT has been individuated. At relatively low NFTs, $L_{10\%}$ decays linearly, and at high NFTs, it is equal to zero. The onset of rapid decay in the middle-range zone depends on the velocity. Therefore, the major influence of the NFT is on the frozen-layer thickness.

NFT RESULTS FOR TWO DIFFERENT SOFTWARE PACKAGES

To appreciate differences between VISI Flow and Moldflow, simulations with PA6 were also carried out in a Moldflow environment. The filled length and the filled length at P_{max} were used to compare

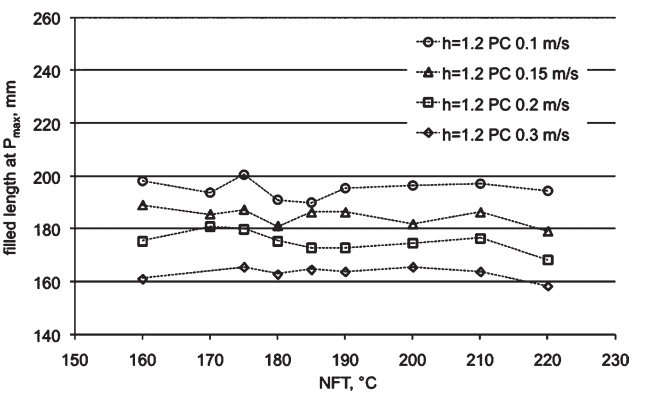

Figure 5 Plot of the filled length at P_{max} (PC, $h = 1.2$ mm).

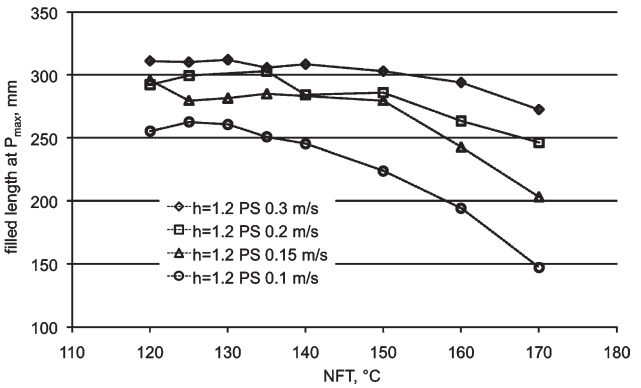

Figure 6 Plot of the filled length at P_{max} (PS, $h = 1.2$ mm).

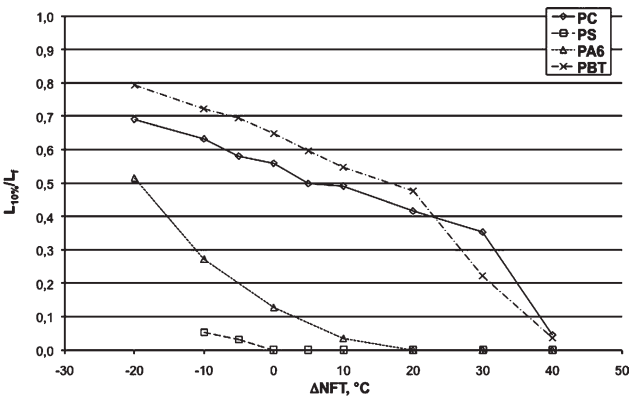

Figure 8 Plot of the length with a frozen layer of 0–10% versus ΔNFT (NFT − NFT_0; $v = 0.2$ m/s, $h = 1.2$ mm).

results. Moldflow predicts $L_{10\%} = 0$ in all cases; therefore, a comparison of packages is not possible with this variable. It is worth noticing that $L_{10\%} = 0$ corresponds to a frozen-layer fraction higher than 10% in the whole mold, even in the zone close to the injection point.

The filled length (Fig. 9) of Moldflow predictions is less than that predicted by VISI Flow, particularly at low NFTs and high velocities. At NFT = 175°C and $v = 0.3$ m/s, the Moldflow filled length is 200 mm less than that predicted by VISI Flow. At high NFTs, differences diminish because of a different dependence on the NFT. Moldflow results do not show appreciable differences with changes in the NFT; conversely, VISI Flow predicts lower values with increasing NFTs.

The filled length at P_{max} is not sensitive to the NFT for the Moldflow or VISI Flow results. The influences on the length and velocity, as predicted by the two packages, are different:

1. VISI Flow: Increasing the injection speed reduces the filled length at P_{max}.
2. Moldflow: Increasing the injection speed increases the filled length at P_{max}.

Although the numerical results are dissimilar, the filled length at P_{max} does not depend on the NFT. By extension, this is a confirmation of the insensitivity of the filling pressure to the NFT.[13] This statement can be physically based on the observation that material properties (e.g., the viscosity), which depend on the temperature and shear rate, and heat-transfer contributions (viscous heating and convection) tend to compensate for the modifications of local conditions induced by changes in the NFT (e.g., the frozen-layer fraction).

VISCOSITY INCREASE AT THE NFT

In the first stage, a correlation between the NFT and viscosity was sought and investigated. A common critical viscosity value was not detectable; nevertheless, the viscosity calculated on the basis of the VISI Flow database exhibited the same order of magnitude within each polymer class. On the other hand, results based on the Moldflow database fell in a wider range covering about 7 orders of magnitude. Therefore, the NFT appears not to be related to an absolute critical value of the apparent viscosity.

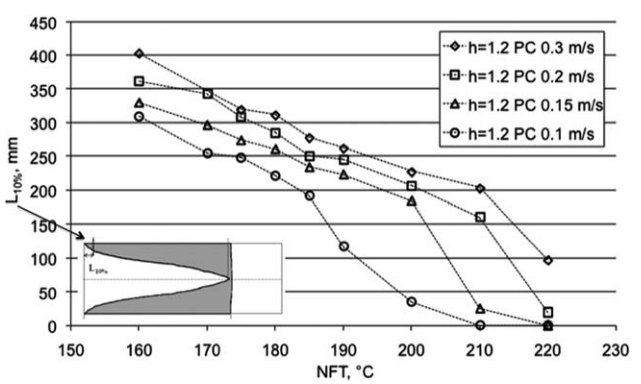

Figure 7 Plot of the length with a frozen layer of 0–10% versus NFT (PC, $h = 1.2$ mm).

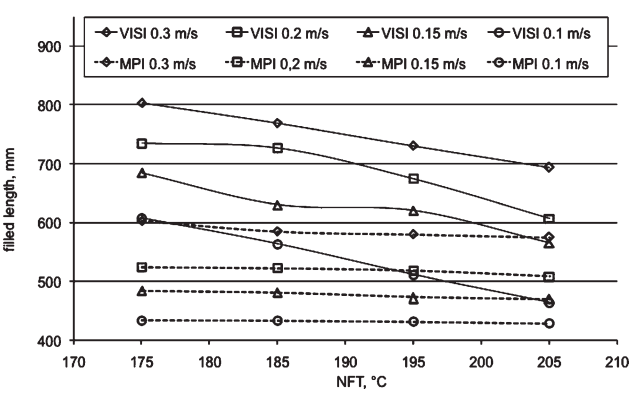

Figure 9 Filled length versus NFT: VISI Flow and Moldflow results.

TABLE III
Cross–WLF Parameters for the Amorphous Polymers Used for the Calculation of (d log η_0)/dT from the VISI Flow Database

	n	τ^* (Pa)	D_1 (Pa s)	D_2 (K)	A_1	A_2 (K)
PC-1	0.2313	5.985×10^5	2.65×10^{15}	417.15	36.789	51.6
PC-2	0.2563	5.78×10^5	1.31×10^{20}	417.15	50.082	51.6
PC-3	0.2126	4.19×10^5	2.98×10^9	417.15	21.113	51.6
PC-4	0.5903	4.06×10^3	1.90×10^{14}	417.15	32.134	51.6
PC-5	0.09	8.97×10^5	7.54×10^{10}	417.15	25.929	51.6
PC-6	0.1143	8.48×10^5	5.17×10^{11}	417.15	28.039	51.6
PC-7	0.17	6.69×10^5	6.03×10^{10}	417.15	25.835	51.6
PMMA-1	0.3747	2.25×10^4	4.76×10^{24}	390.15	65.83	51.6
PMMA-2	0.3524	5.67×10^4	2.87×10^{14}	377.15	34.387	51.6
PMMA-3	0.3192	1.02×10^5	1.43×10^{16}	377.15	40.301	51.6
PMMA-4	0.2664	1.19×10^5	9.39×10^{16}	377.15	43.03	51.6
PMMA-5	0.3474	5.29×10^4	1.19×10^{12}	377.15	27.893	51.6
PMMA-6	0.2368	1.23×10^5	2.33×10^{17}	377.15	44.038	51.6
PMMA-7	0.2808	1.83×10^4	2.53×10^{27}	377.15	69.836	51.6
PS-1	0.2985	2.34×10^4	7.29×10^{12}	373	30.71	51.6
PS-2	0.3188	1.88×10^4	9.94×10^8	373.15	18.22	51.6
PS-3	0.3082	2.33×10^4	2.55×10^{10}	373.15	19.458	51.6
PS-4	0.2435	4.35×10^4	1.42×10^{10}	373.15	19.282	51.6
PS-5	0.334	6.71×10^3	5.55×10^{18}	323.15	41.667	51.6
PS-6	0.3779	4.29×10^4	3.28×10^8	373.15	23.379	51.6
PS-7	0.3011	1.44×10^4	3.41×10^{13}	373.15	29.596	51.6
PS-8	0.2233	3.70×10^4	1.56×10^{15}	323.15	35.383	51.6
PS-9	0.3359	3.26×10^3	3.32×10^{12}	373.15	24.27	51.6
PS-10	0.2577	3.08×10^4	5.03×10^9	373.15	21.532	51.6

From a dynamic perspective, the NFT can be connected to a critical variation in the viscosity, which causes the set-in of no-flow conditions. Because a critical viscosity value cannot be related to the NFT, critical melt hardening can better characterize the flow stopping during filling. This means that flow stopping is related to the dependence of the viscosity on temperature, and below the NFT, the viscosity increase is so high that the flow rate becomes negligible.

With reference to the zero-shear viscosity, values of $d\eta_0/dT$ can provide an estimate of the increase in the viscosity caused by temperature lowering. This parameter is related to absolute changes and therefore can be different for different classes of polymers. Normalization of $d\eta_0/dT$ with η_0 leads to (d log η_0)/dT, a parameter with the dimension K^{-1} suitable for quantifying the relative increase in the viscosity caused by temperature lowering.

The rheological model most widely adopted by commercial software packages is the Cross–WLF model:[25]

$$\eta(T,\dot{\gamma}) = \frac{\eta_0(T)}{1 + \left(\frac{\eta_0(T)\dot{\gamma}}{\tau^*}\right)^{1-n}} \tag{2}$$

where T is the temperature, $\dot{\gamma}$ is the shear rate, i.e. the velocity gradient dv/dx, and τ^* is the critical shear stress value. $\eta_0(T)$ the zero-shear-viscosity, is calculated as follows:

$$\eta_0(T) = D_1 \exp\left[-\frac{A_1(T - D_2)}{A_2 + (T - D_2)}\right] \tag{3}$$

where A_1, A_2, D_1, D_2, and n are material parameters.

From eq. (3), we can work out the following expression:

$$\left.\frac{d\log\eta_0}{dT}\right|_{T=\mathrm{NFT}} = -\frac{A_1A_2}{[A_2 + (\mathrm{NFT} - D_2)]^2} \tag{4}$$

This represents the relative increase in the viscosity at T = NFT. With the material parameters (A_1, A_2, D_1, and D_2) reported in the package databases (Table III), values of (d log η_0)/dT were calculated and compared.

Results and discussion

For various amorphous polymers, such as PCs, PSs, and poly(methyl methacrylate)s (PMMAs), the values obtained from the VISI Flow database are quite comparable (Fig. 10), except for a few cases. T_g was introduced as a shift factor so that we could compare the results of different types of materials on a common basis. Values are reported in Table IV. These values were obtained via extrapolation because T_g depends on the actual cooling rate.

Therefore, values of (d log η_0)/dT were averaged for each material type, and the NFT for each

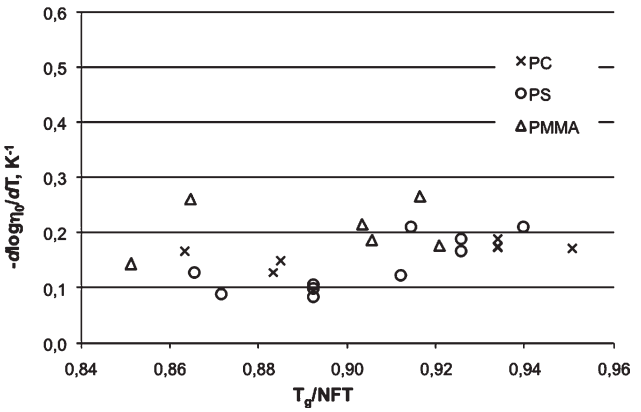

Figure 10 $(d \log \eta_0)/dT$ versus T_g/NFT calculated from the VISI Flow database for amorphous materials.

material was then recalculated via eq. (4) with the averaged value. The calculation results are displayed in Tables V–VII.

The conclusions that can be drawn from these simple computations are as follows:

- The differences between NFTs reported in the software package databases and those estimated via $(d \log \eta_0)/dT$ are not significant for PC.
- PMMA and PS show greater differences but large ΔNFT values (30–40°C) in only a few cases.
- The evaluation of $(d \log \eta_0)/dT$ can be successfully used for a first estimate of the NFTs of amorphous polymers.

Different results were obtained when the parameters of the Moldflow database were chosen (Fig. 11). It has to be underlined that the NFT values are different in the two databases: for example, the NFT of PC MK2600 is 180°C in the VISI Flow database and 150°C in the Moldflow database. This large difference is due to the different typologies of the experimental setups used to determine the NFTs. Presumably, the VISI Flow measurements were carried out under shear, whereas the Moldflow measurements were performed under static conditions, e.g. via DSC. Moreover, the parameters of the Cross–WLF equation for the same material are slightly different in the two databases.

TABLE IV
T_g Values of the Amorphous Materials

Material	T_g (°C)
PC	150
PS	100
PMMA	110

TABLE V
NFTs, $(d \log \eta_0)/dT$ Values, NFTs Recalculated from Average $(d \log \eta_0)/dT$ Values, and Corresponding ΔNFTs for Different PCs

	NFT (°C)	$[(d \log \eta_0)/dT]_{T=\mathrm{NFT}}$	NFT recalculated (°C)	ΔNFT (°C)
PC-1	205	−0.150	200	5
PC-2	217	−0.167	218	−1
PC-3	172	−0.173	174	−2
PC-4	206	−0.129	193	13
PC-5	180	−0.175	183	−3
PC-6	180	−0.189	186	−6
PC-7	180	−0.174	182	−2
Average		−0.165		

To check values of $(d \log \eta_0)/dT$, the values from the VISI Flow database were used as reference values, and the NFTs of the Moldflow database were increased by 30°C (according to the rule of thumb reported in the introduction[18]). Figure 11 summarizes the result of this manipulation with a constant T_g value used as a shift factor (Table II): the Moldflow (Moldflow Plastics Insight, MPI) values practically superimpose to the VISI Flow values.

The assumption of a constant T_g value for each type of polymer is merely qualitative because it depends on various parameters (e.g., the molecular weight). The choice of a constant T_g value was due to the lack of T_g values in the VISI Flow and Moldflow databases. This approximation leads to a cloud of points with $T_g/\mathrm{NFT} > 1$, that is, $\mathrm{NFT} < T_g$. It is worth noticing that this is physically incorrect because the NFT has to be at least equal to T_g.

A qualitative inspection of Figure 11 shows a narrow range of $-(d \log \eta_0)/dT$ values for $T_g/\mathrm{NFT} < 0.95$ and a wide range for $T_g/\mathrm{NFT} > 0.95$. This suggests that for NFTs higher than T_g, the assumption of a constant $(d \log \eta_0)/dT$ value can consistently depict the NFT phenomenology.

Similar calculations were performed for five classes of semicrystalline materials: polypropylene, poly(ethylene terephthalate) (PET), PBT, PA6, and

TABLE VI
NFTs, $(d \log \eta_0)/dT$ Values, NFTs Recalculated from Average $(d \log \eta_0)/dT$ Values, and Corresponding ΔNFTs for Different PMMAs

	NFT (°C)	$[(d \log \eta_0)/dT]_{T=\mathrm{NFT}}$	NFT recalculated (°C)	ΔNFT (°C)
PMMA-1	135	−0.704	176	−41
PMMA-2	150	−0.187	132	18
PMMA-3	151	−0.215	139	12
PMMA-4	177	−0.143	142	35
PMMA-5	143	−0.176	124	19
PMMA-6	145	−0.266	143	2
PMMA-7	170	−0.261	166	4
Average		−0.279		

TABLE VII
NFTs, $(d \log \eta_0)/dT$ Values, NFTs Recalculated from Average $(d \log \eta_0)/dT$ Values, and Corresponding ΔNFTs for Different PSs

	NFT (°C)	$[(d \log \eta_0)/dT]_{T=NFT}$	NFT recalculated (°C)	ΔNFT (°C)
PS-1	135	−0.211	154	−19
PS-2	136	−0.123	130	6
PS-3	155	−0.089	133	22
PS-4	145	−0.107	133	12
PS-5	145	−0.100	122	23
PS-6	124	−0.212	141	−17
PS-7	158	−0.128	153	5
PS-8	145	−0.085	112	33
PS-9	130	−0.189	143	−13
PS-10	130	−0.168	137	−7
Average		−0.141		

polyamide 46 (PA46). Results are reported in Figures 12 and 13. Surprisingly, even in this case, a narrow range of $(d \log \eta_0)/dT$ values was found with both the VISI Flow and Moldflow databases for all the materials considered, except for a few cases (especially PET and PBT). This similarity of results for semicrystalline polymers is due to the low differences in the NFT values reported by the VISI Flow and Moldflow databases (ca. 10°C) and to the very close (or equal in many cases) viscosity parameters. Most of the points lie within the range of $0.05 < (d \log \eta_0)/dT < 0.1$; this range is lower than that for amorphous materials and thus indicates that in semicrystalline polymers, the NFT is associated with a smaller change in the relative viscosity versus amorphous polymers.

In principle, if the $(d \log \eta_0)/dT$ criterion has general validity, with the addition of the contribution of the viscosity enhancement due to crystallization to

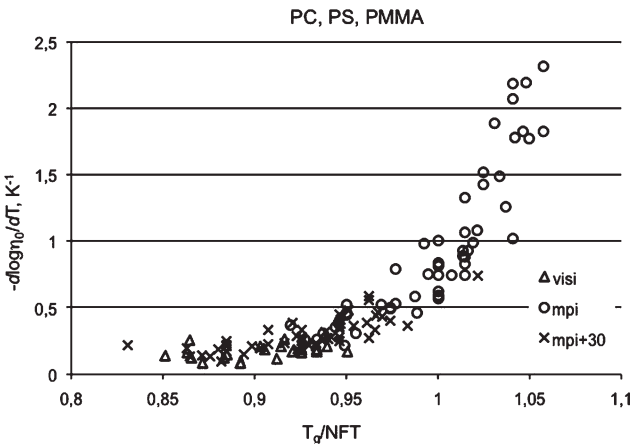

Figure 11 $(d \log \eta_0)/dT$ versus T_g/NFT calculated from the VISI Flow database, Moldflow database, and a modification of the Moldflow database for amorphous materials.

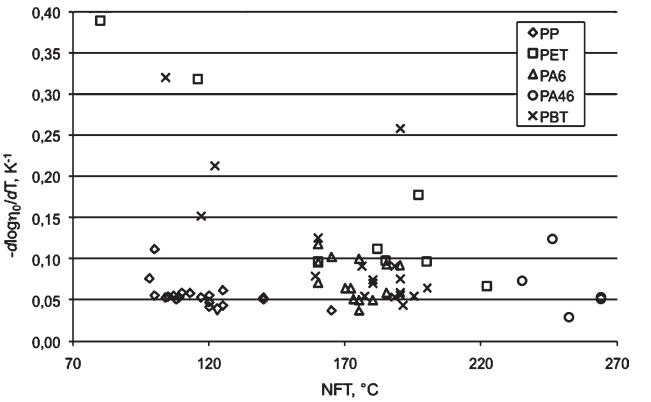

Figure 12 $(d \log \eta_0)/dT$ versus NFT calculated from the VISI Flow database for semicrystalline materials.

$(d \log \eta_0)/dT$, values closer to those of amorphous materials should be achieved.

The NFT is a parameter independent of processing conditions. Conversely, the proposed one represents a hardening velocity. In addition to gelation, for which solidlike behavior depends on the time of observation, $(d \log \eta_0)/dT$ coupled with dT/dt can produce a typical hardening time and thus highlights how thermal history affects the solidification dynamics.

CONCLUSIONS

The NFT, despite its simple definitions and use in injection molding simulations, remains an open issue for improving the performance and the prediction capabilities of computer-aided engineering packages.

The NFT is a useful parameter for speeding up the computational time and overcoming the lack of accuracy of viscosity models in low-temperature regions. It certainly plays a key role in the prediction of frozen-layer evolution and set-in and therefore in

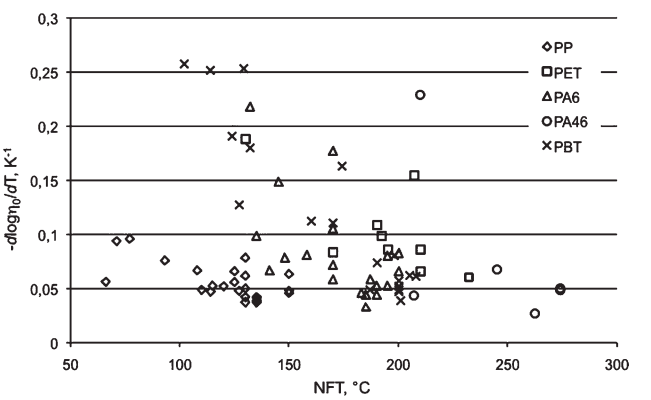

Figure 13 $(d \log \eta_0)/dT$ versus NFT calculated from the Moldflow database for semicrystalline materials.

estimating the performance, long-term stability, and failure of injection-molded parts, as demonstrated by the effect of the NFT on the mold-filling length (short shots). The use of the NFT is extended further as a way of determining whether residual stresses[26] will accumulate or relax at a particular node; this is the starting point for the subsequent estimation of shrinkage and warpage.[27] Moreover, models for the prediction of shrinkage and warpage need further improvement, and to accomplish this result, a more precise definition and a deeper characterization of the NFT will play a fundamental role.

The complexity of studies concerning the NFT stems also from the patented technology of software packages, which limits the global understanding of the mechanisms influencing NFT-related phenomena. Further difficulties are related to the variety of methods for estimating the NFT in different software packages; for example, Moldflow uses different ways to measure NFT, and even DSC characterizations are normally carried out at three different cooling rates much lower than the actual cooling rates in injection molding.

The physical phenomena that determine where (across the melt thickness) the transition between the flowing melt and the stagnant melt occurs are still unclear, and surely they are different for amorphous and semicrystalline polymers. For semicrystalline polymers, a relationship between the NFT and physical gelation is reasonable, but studies on gelation are still in progress. Improvements of software predictions are also related to viscosity models; these so far have not taken into account crystallization effects, which are highly relevant for semicrystalline materials. Therefore, an improvement of NFT characterization must be coupled with developments in viscosity models to reach better agreement between simulations and experiments.

First, definitions of the NFT must be better specified. A correlation with $(d \log \eta_0)/dT$ shows good agreement for both amorphous and semicrystalline polymers, so this way should be deeply investigated for thorough validation. For amorphous materials, the value of $(d \log \eta_0)/dT$ is approximately 0.2 K^{-1}, whereas for semicrystalline materials, it is approximately 0.05 K^{-1}. These different values can be related to the different phenomena occurring in the two cases, although viscosity models do not take into account this issue. Moreover, alternative correlations and modeling of the NFT have been checked without fulfilling results.[28]

A sensitivity analysis has shown many interesting aspects. First, running similar simulation in different software environments leads to very different results. Moreover, with changes in software packages, the NFT exhibits different sensitivities to the same parameters.

A general result is that the main influence of the NFT is on the frozen layer. All things considered, the NFT is expected to show a larger influence on the holding stage than on the filling stage. Therefore, a study about the influence of the NFT on the holding stage is needed to properly understand its role in shrinkage and warpage prediction. Moreover, models for shrinkage (and especially warpage) prediction must be improved because they fail with respect to accuracy many times.

The NFT shows a slight influence on the filled length in a short shot and a negligible influence on the filled length at P_{max}. As a result, the NFT does not appreciably influence pressure predictions.

To improve the accuracy of injection molding simulations, a more accurate characterization of the NFT is mandatory. Because many aspects of injection molding simulations are still improving, (e.g., the influence of crystallization[29] and the prediction of warpage[30]), such aspects being directly related to the NFT, the progress in the accuracy of injection-molding simulations is connected in some way to the phenomena concerning NFT.

References

1. Wong, H. Y.; Fung, K. T.; Gao, F. Sens Actuators A 2008, 141, 712.
2. He, B.; Zhang, X.; Zhang, Q.; Fu, Q. J Appl Polym Sci 2008, 107, 94.
3. La Carrubba, V.; Gabrielse, W.; van Gurp, M.; Piccarolo, S.; Brucato, V. J Appl Polym Sci 2003, 89, 3713.
4. Winter, H. H.; Mours, M. Adv Polym Sci 1997, 134, 165.
5. Pogodina, N. V.; Winter, H. H.; Srinivasm, S. J Polym Sci Part B: Polym Phys 1999, 37, 3512.
6. Pogodina, N. V.; Lavrenko, V. P.; Srinivas, S.; Winter, H. H. Polymer 2001, 42, 9031.
7. Coppola, S.; Acierno, S.; Grizzuti, N. Macromolecules 2006, 39, 1507.
8. Lamberti, G.; Peters, G. W. M.; Titomanlio, G. Int Polym Process 2007, 22, 303.
9. Acierno, S.; Coppola, S.; Grizzuti, N.; Maffettone, P. L. Macromol Symp 2002, 185, 233.
10. Titomanlio, G.; Speranza, V.; Brucato, V. Int Polym Process 1997, 12, 45.
11. Kamal, M. R.; Kenig, S. Polym Eng Sci 1972, 12, 302.
12. Richardson, S. M. Rheol Acta 1983, 22, 223.
13. Kennedy, P. K. Flow Analysis Reference Manual; Hanser: Munich, 1993.
14. Cox, H. W.; Mentzer, C. C.; Custer, R. C. Polym Eng Sci 1984, 24, 501.
15. DataPointLabs. Test Report: Alcryn 2070bk. http://www.apainfo.com/Download.asp?PDF=pdf/Alcryn%202070BK%20-Mold%20Flow%20Analysis.pdf (accessed June 2010).
16. Struik, L. C. E. Physical Aging in Amorphous Polymers and Other Materials; Elsevier: Amsterdam, 1978.
17. He, J.; Zoller, P. J Polym Sci Part B: Polym Phys 1994, 32, 1049.
18. Bok Lee, Y.; Hun Kwon, T.; Yoon, K. Polym Eng Sci 2002, 42, 2246.
19. Ryan, A. J. Emerging Themes in Polymer Science; Royal Society of Chemistry: London, 2001.
20. Janeschitz-Kriegl, H. Rheol Acta 1977, 16, 327.
21. Janeschitz-Kriegl, H. Rheol Acta 1979, 18, 693.

22. Eder, G.; Janeschitz-Kriegl, H.; Liedauer, S. Prog Polym Sci 1990, 15, 629.
23. Kennedy, P. K. Ph.D. Thesis, Technical University of Eindhoven, 2008.
24. Andersson, P. Ph.D. Thesis, Linkpings Universitet, 2002.
25. Han, C. D. Rheology and Processing of Polymeric Materials; Oxford University Press: Oxford, 2007; Vol. 1.
26. Isayev, A. I.; Hieber, C. A.; Crouthamel, D. L. SPE Tech Pap 1981, 27, 110.
27. TestPaks. No-Flow Temperature in Mold Analysis. http://www.testpaks.com/news73.htm#5 (accessed June 2010).
28. Mannella, G.; La Carrubba, V. Characterization of No-Flow Temperature of Semi-Crystalline Materials; DSM Research Internal Report: Geleen, The Netherlands, 2008.
29. Pantani, R.; Coccorullo, I.; Speranza, V.; Titomanlio, G. Prog Polym Sci 2005, 30, 1185.
30. Fischer, J. M. Handbook of Molded Part Shrinkage and Warpage; Plastics Design Library: Norwich, NY, 2003.